

This is an Open Access document downloaded from ORCA, Cardiff University's institutional repository: <https://orca.cardiff.ac.uk/id/eprint/122648/>

This is the author's version of a work that was submitted to / accepted for publication.

Citation for final published version:

Pont, Sebastian, Osella, Silvio, Smith, Alastair, Marsh, Adam V., Li, Zhe, Beljonne, David, Cabral, João T. and Durrant, James R. 2019. Evidence for strong and weak phenyl-C61-butyric acid methyl ester photodimer populations in organic solar cells. *Chemistry of Materials* 31 (16) , pp. 6076-6083. 10.1021/acs.chemmater.8b05194

Publishers page: <http://dx.doi.org/10.1021/acs.chemmater.8b05194>

Please note:

Changes made as a result of publishing processes such as copy-editing, formatting and page numbers may not be reflected in this version. For the definitive version of this publication, please refer to the published source. You are advised to consult the publisher's version if you wish to cite this paper.

This version is being made available in accordance with publisher policies. See <http://orca.cf.ac.uk/policies.html> for usage policies. Copyright and moral rights for publications made available in ORCA are retained by the copyright holders.



Evidence for strong and weak PCBM photo-dimer populations in organic solar cells

Sebastian Pont,^{a,b} Silvio Osella,^c Alastair Smith,^b Adam Marsh,^{a,b} Zhe Li,^d David Beljonne,^c João T Cabral,^{a,e} James R Durrant^{a,b,f}

In polymer / fullerene organic solar cells, the photochemical dimerisation of PCBM was reported to have either beneficial or detrimental effect on device performance and stability. In this work, we investigate the behavior of such dimers by measuring the temperature dependence of the kinetics of PCBM de-dimerisation as a function of prior light intensity and duration. Our data reveal the presence of both 'weakly' and 'strongly' bound dimers, with higher light intensities preferentially generating the latter. DFT simulations corroborate our experimental findings and suggest a distribution of dimer binding energies, correlated with the orientation of the fullerene tail with respect to the dimer bond on the cage. These results provide a framework to rationalize the double-edged effects of PCBM dimerization on the stability of organic solar cells.

1 Introduction

To realise the growing potential of organic solar cells (OSC), improvements in operational stability remains a key challenge.¹ The development of new polymers and acceptors is continuing to increase the efficiency of OSC.²⁻⁴ The current record certified power conversion efficiency is over 17%⁵, achieved in a tandem device architecture incorporating fullerene and non-fullerene electron acceptors. However, the potential loss of OSC power conversion efficiency over time is a key concern for commercialization. This loss can be caused by various stresses factors. Environmental elements such oxygen and humidity can react with materials within the device; these factors may be encapsulated against in certain applications, such as those employing glass encapsulation. However, intrinsic factors such as thermal stress, illumination, and interlayer-stability cannot be encapsulated against and therefore are always present during operation.⁶⁻⁸ In particular, OSC are often observed to undergo significant light induced degradation during the initial stages of operation known. This is termed the 'burn-in' and is related to several loss mechanisms which are current areas of interest.⁹⁻¹¹ Other studies have highlighted the potential for thermally induced degradation of performance, often associated with changes in film morphology.¹²⁻¹⁴ The light induced dimerization of the most widely used, fullerene based, electron acceptor PCBM (*phenyl-C₆₁-butyric-acid-methyl ester*) was reported to be a factor in both of these intrinsic degradation pathways, in some cases detrimentally^{15,16} as the under-

lying cause of device 'burn-in', in other cases beneficially¹⁷⁻¹⁹ in improving film morphological stability. In this study, we focus on these apparently contradictory effects of PCBM dimerization, and in particular provide evidence that light irradiation can result in the formation of two distinct populations of PCBM dimers depending upon the irradiation conditions used.

The dimerisation of fullerenes in OSC bulk heterojunctions is known to occur during operating conditions.¹⁵⁻¹⁷ The photochemical mechanism of PCBM dimerisation has also been correlated with beneficial effects due to improved morphology stability in a number of polymer:fullerene systems.¹⁷⁻¹⁹ PCBM crystallisation is one of the key causes of morphological degradation under thermal stress; the formation of PCBM dimers unit was suggested to impede the nucleation of such PCBM crystallites, thereby enhancing film and device stability.¹⁷ The dimer is also immobile compared to the monomer unit.¹⁹ However, other reports have suggested neutral or detrimental effects of PCBM dimerisation on the performance and stability of OSCs. Distler et al reported that dimerisation was correlated with the formation of trap-states during the degradation of PDTSTzTz:PCBM devices.¹⁵ More recently, Heumueller et al presented further examples of PCBM dimerisation causing device degradation in seven different polymer:fullerene material systems.¹⁶ However, Inasaridze et al have observed no burn-in within systems where PCBM dimerisation is occurring, and systems with burn-in without dimerisation.²⁰ From these results, it is clear the effect of fullerene dimerisation on stability is non-trivial and the current models in the literature present conflicting conclusions.

The first study of the photochemical dimerisation of C₆₀ was reported 20 years ago by Rao et al.²¹ This 2+2 cycloaddition reaction was proposed to be driven by photogenerated fullerene triplet states.²² The dimerisation was observed in other fullerenes, such as C₇₀ and PCBM, but at slower rates of formation, attributed to asymmetry and steric hindrance effects.^{23,24}

^a Centre for Plastic Electronics, Imperial College London, London, SW7 2AZ.

^b Department of Chemistry, Imperial College London, London, SW7 2AZ.

^c Center for Research in Molecular Electronics and Photonics, University of Mons, 7000 Mons, Belgium.

^d School of Engineering, Cardiff University, Cardiff, CF10 3AT

^e Department of Chemical Engineering, Imperial College London, London, SW7 2AZ.

^f College of Engineering, Swansea University, Bay Campus, SA1 8EN.

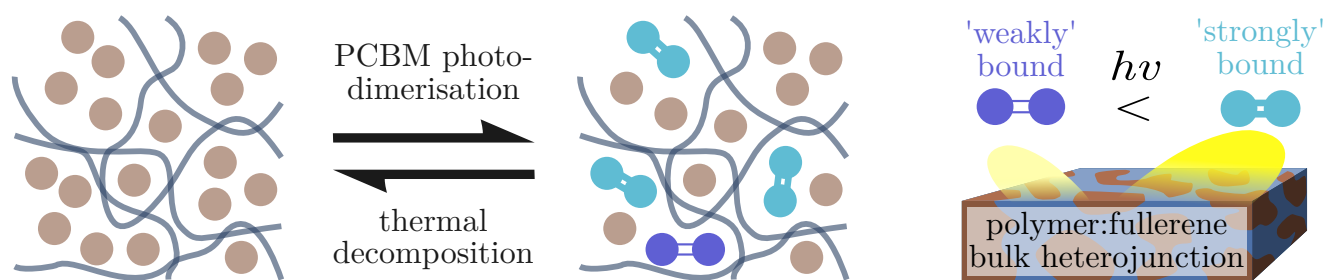


Figure 1 Upon illumination PCBM undergoes a 2+2 cycloaddition reaction to form dimers. These are thermally reversible at elevated temperatures. In polymer:fullerene bulk heterojunctions distinct dimer populations are found to occur that have varying stability to de-dimerisation. This is associated with the configuration of the asymmetric PCBM units in the dimers. At high light irradiances predominately 'strong' dimers are formed whereas at lower light intensities 'weak' PCBM dimers are formed. These results present a pathway to understand the simultaneous beneficial and detrimental effects of PCBM dimerisation in OSCs.

The topological criteria for dimerization is the alignment of two carbon-carbon double bonds at a separation of less than 4.2 Å. In crystalline PCBM, this requirement is met, with a fullerene cage separation of 3.5 Å. Conversely, PCBM crystallization was reported to lower the yield of long-lived triplet states.²⁵ Temperature dependence studies on C₆₀ shows it freely rotates about its centre of mass at and above room temperature.²⁶ Although there are many criteria for dimerisation, the 30 × 30 = 900 possible orientations have been suggested to aid with the relatively high yields of dimerization in neat C₆₀ films.²⁷ For C₆₀, thermally induced de-dimerisation was observed, with an activation energy of 1.25 eV.²⁶ The de-dimerisation in PC₆₀BM dimers was studied by Wong et al.¹⁸ The reaction kinetics are found to be very similar to C₆₀, with an activation energy of 0.96 eV.

To study the kinetics of PCBM dimerisation an absorbance assay was used to probe the fraction of dimers to monomers.^{15,16} This facile assay enables time-resolved monitoring of the PCBM dimerisation and de-dimerisation. A representative bulk heterojunction of PCDTBT:PCBM thin films were exposed to varying duration and intensity of light exposure followed by dark thermally annealing. By analyzing the kinetics of the thermal de-dimerisation the resulting PCBM dimer bond energies are correlated with light intensity and duration. This work will present a framework to understand the conflicting effects of PCBM dimerisation in OSC and strategies to maximize both performance and stability.

2 Results and Discussion

2.1 Distinct dimer populations

In this study, the kinetics of thermally induced PCBM de-dimerisation are probed in polymer:fullerene blends in order to investigate the energetic distribution of dimer bond strengths. Previous studies have probed the yields of de-dimerisation using gel permeation chromatography (GPC) or high-performance liquid chromatography (HPLC).^{15,16,18} As these techniques require destruction of the sample time-resolved measurements are not feasible. Recently, it was shown that the relative proportions of PCBM monomer and dimer states can be readily assayed from UV/visible absorption spectroscopy.^{15,19} This absorbance

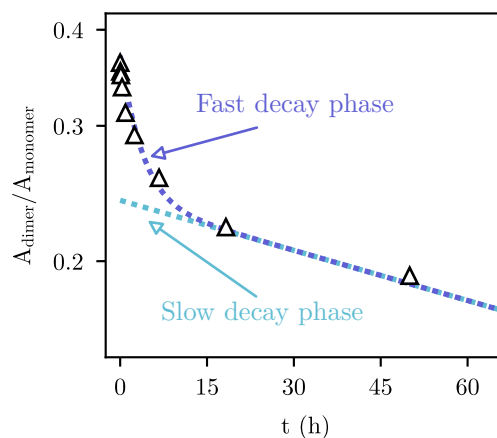


Figure 2 The PCBM dimer:monomer ratio of a PCDTBT:PCBM 1:2 thin film whilst annealing at 100 °C in the dark. The film had prior illumination at 186 W m⁻² for 82 h which resulted in the PCBM dimer concentration at $t = 0$ min. Two phases of de-dimerisation are observed: firstly, a fast-phase with rate of $\approx 181 \text{ min}^{-1}$ upon which the 'weakly' bound dimers separate and, secondly, a slow-phase with a rate of $\approx 12.6 \times 10^3 \text{ min}^{-1}$ where 'strongly' bound dimers separate.

assay facilitates collecting time-resolved dimer concentrations, enabling analysis of the kinetics of PCBM dimerisation and de-dimerisation, as detailed below.

To investigate the de-dimerisation kinetics, PCDTBT:PCBM films were initially irradiated with a white light LED (with negligible UV light, see Figure S1 for spectrum) to induce partial PCBM dimerisation, and then annealed at 100 °C in the dark to induce de-dimerisation. Absorbance spectra were taken periodically while annealing to monitor the kinetics of de-dimerisation. Specifically, the change in an absorbance feature at 320 nm was converted to a dimer:monomer ratio using a previously reported calibration.^{ref other paper} Figure 2 presents dimer population decay over time following prior irradiation at 186 W m⁻² for 82 h. Complete reversibility of the photo-dimerisation has previously been shown to occur in this system and therefore expected to occur here at very long timescales.^{18,26} It was expected that the de-

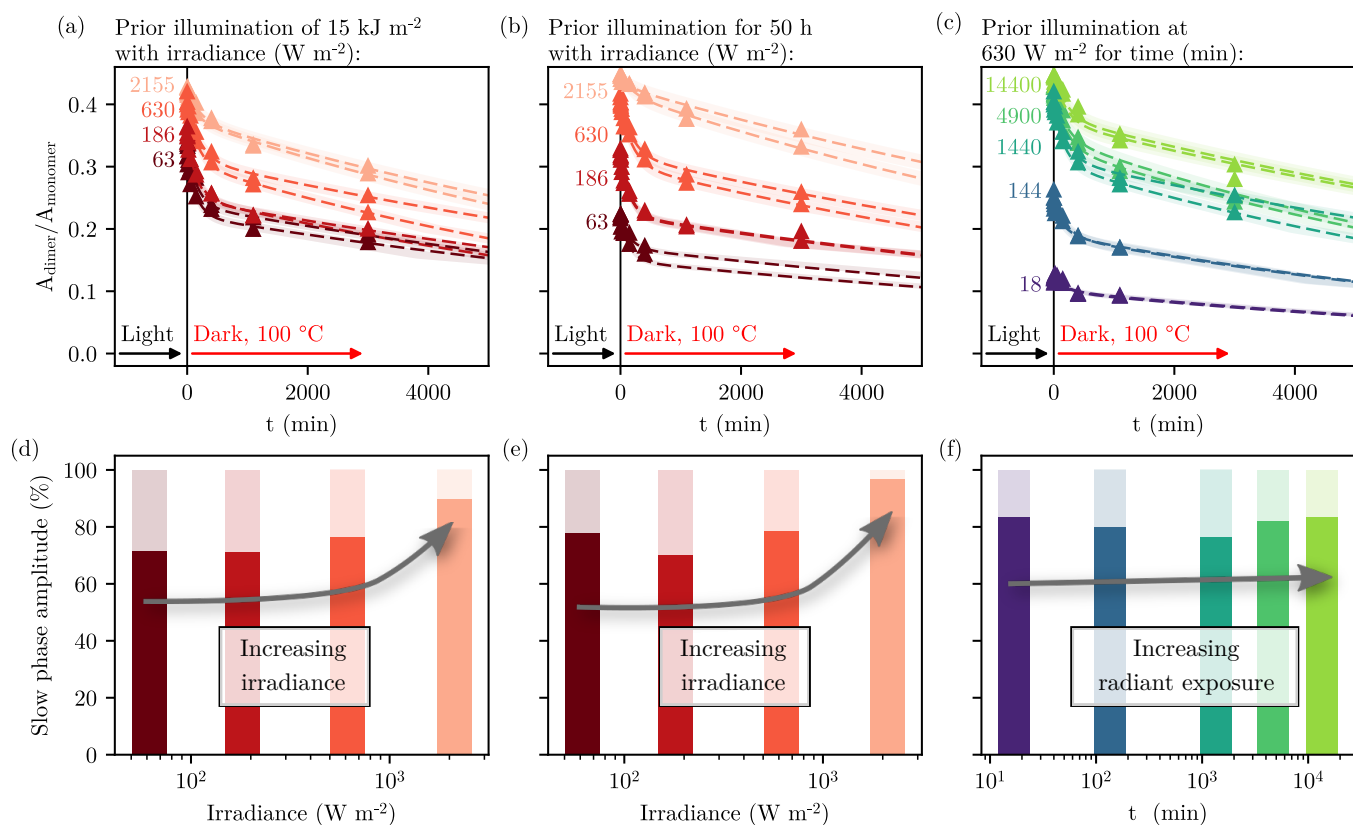


Figure 3 (a-c) PCBM dimer:monomer ratio in PCDTBT:PCBM thin films whilst annealing at 100 °C in the dark with prior illumination with three scenarios: (a) equal radiant exposure, (b) equal illumination time, and (c) equal irradiance. For each measurement repeats are presented as separate markers. Fitting of the two-phase decay gives the amplitude of the fast-phase and the slow-phase after the illumination. (d-f) The percentage of the slow-phase formed for the various conditions. These results show the amount of slow-phase is dependent on irradiance, and not radiant exposure or illumination time.

decay would follow the reaction model described by Eklund et al and used in previous analyses of the de-dimerisation kinetics.¹⁸ This model states the dimer concentration, D , should exhibit a (mono-exponential) decay over time upon isothermal annealing, following where $D(t) = D(t_0) \exp(-kt)$ at time t and decay rate k . However, a mono-exponential decay does not fit the data in Figure 2. Empirically, we find that a bi-exponential decay describes all data in full:

$$D(t) = D_{\text{slow}} \exp(-k_{\text{slow}}t) + D_{\text{fast}} \exp(-k_{\text{fast}}t) \quad (1)$$

where D is dimer concentration at time t , D_{slow} and D_{fast} are termed the slow- and fast-phase, respectively, and k_{slow} and k_{fast} are the associated decay rate constants, respectively. Several possible interpretations can be considered for this behaviour. Fullerenes have been shown to oligomerize²¹ and the formation of PCBM trimers was reported by several groups (e.g.¹⁸); these could contribute to an additional time decay profile. Alternatively, the dimerization process itself could be non-exponential (e.g. described an stretched exponential) potentially associated with matrix rearrangements required for thermal decomposition to occur; however, we find that a bi-exponential description provides better agreement with experiment. Given that the light spectrum has a broad frequency range, one could conceivably ac-

cess different reaction and thus dimer pathways depending on incident light energy; however, no wavelength-dependence in dimerisation was reported in PCBM films.²⁴ Finally, we hypothesize that the intrinsic distribution of relative spatial configurations of PCBM molecules with a film might result in the formation of distinct photo-dimers, which could then be expected to exhibit different de-dimerization energetic requirements and thus kinetics. Some evidence for dimer complexity is suggested by structured HPLC traces upon light exposure and re-dissolution. Next, we experimentally investigate the role of light intensity and time (and thus radiant exposure, or dose) on the de-dimerisation time profile to examine this bi-exponential behavior, and then report on a theoretical examination of dimer topology.

2.2 Reaction kinetics of fast and slow decays

The factors determining the ratio of fast- to slow-phase were investigated by controlling the dimerization illumination conditions prior to annealing. Specifically, three parameters are investigated: the radiant exposure (total energy dose), the irradiance (light intensity), and duration of the light exposure. Firstly, to probe the effect of radiant exposure, PCDTBT:PCBM films were exposed to a constant 15 kJ m⁻² from a white light LED array whilst the irradiance was varied from 63 W m⁻² to 2155 W m⁻². Secondly, to

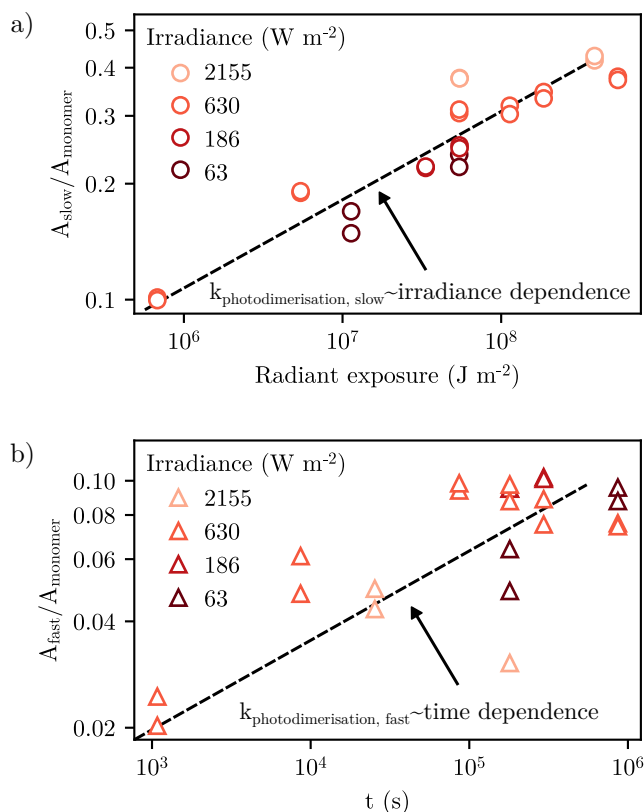


Figure 4 (a) The fraction of the slow decay to total dimerisation correlated against prior radiant exposure. This suggests the reaction follows the expected triplet mechanism previously reported for PCBM dimerisation. (b) The fraction of the fast decay to total dimerisation correlated against prior illumination exposure time. This suggests that even at the lowest irradiance used ($63 W m^{-2}$) the rate of formation is not limited by the illumination.

probe the effect of irradiance, films were illuminated for 50 h with irradiances of $63 W m^{-2}$ to $2155 W m^{-2}$. Lastly, to probe the time dependence, films were exposed to $630 W m^{-2}$ with a duration of 18 min to 14400 min. After light soaking films were annealed at $100^\circ C$ in the dark and absorbance measurements taken intermittently to monitor the de-dimerisation, as in Figure 2. The results of these three conditions are presented in Figure 3(a-c). The decay of the dimer population was fitted with Equation 1. After fitting with the least-squares error, $k_{slow} = 0.135(23) \times 10^{-5} s^{-1}$ and $k_{fast} = 9.31(99) \times 10^{-5} s^{-1}$ to one standard deviation for all the decays in Figure 3(a-c). As such, we can conclude that the dissociation kinetics of the two separate dimers populations are independent of light irradiation conditions, with differences in overall decay kinetics as a function of light irradiation conditions resulting only from variations in the relative magnitudes of the fast and slow de-dimerisation phases.

The previously reported rate of de-dimerisation in PCDTBT:PCBM was $2.28 \times 10^{-5} s^{-1}$ which is between the values of the slow and fast kinetics observed here.¹⁸ The percentage of slow-phase to total dimer ($D_{slow}/[D_{slow} + D_{fast}]$) is plotted in Figure 3(d-f). Figures 3(d) and 3(e) show that illumination

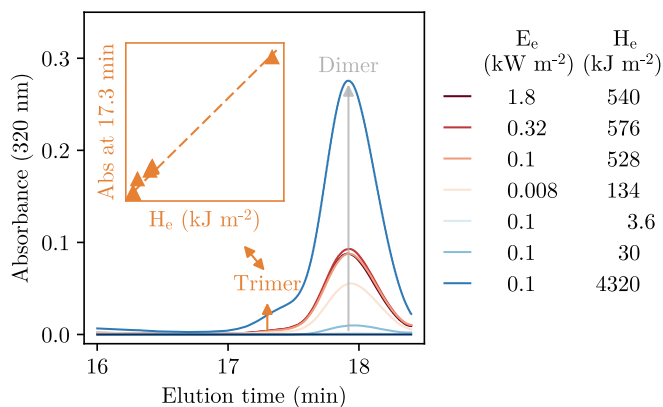


Figure 5 PCBM trimers are observed in PCDTBT:PCBM films which are identified by a shoulder at 17.3 min in the GPC measurements. The inset shows the linear correlation of trimerisation with radiant exposure, H_e . The red traces have similar radiant exposure ($\approx 550 kJ m^{-2}$) with irradiances from $0.1 kW m^{-2}$ to $1.8 kW m^{-2}$ and all form approximately the same concentration of dimer; therefore the trimer formation is independent of the irradiance, E_e . This is different to the trend observed between the strong and weak dimer (E_e dependence) thus the different dimers are not dimer and trimer formation.

at a higher irradiance causes a greater fraction of slow-phase, independent of the radiant exposure or duration of light soaking. In Figure 3(f), the fraction of slow-phase is independent of illumination duration. The fraction of fast- to slow-phase is therefore dependent on the irradiance of illumination, and not the duration of illumination or the radiant exposure. From these measurements, it can be concluded that a key factor controlling the distinct populations is the irradiance. Its underlying mechanism was investigated by analyzing the absolute yield of the slow- and fast-phase. The amplitude of each decay phase (as calculated from Figure 3) was compared with the light duration and with the radiant exposure. Figure 4(a) shows the slow-phase correlates the radiant exposure. This follows the expected trend whereby increasing the illumination duration increases the yield of dimers, independent of intensity. However, the fast-phase correlates with the duration of light exposure, and not with the radiant exposure (Figure 4(b)). This is understood as even at the lowest irradiance investigated ($63 W m^{-2}$) the illumination is not limiting the formation of the fast-phase. Therefore, increasing the irradiance does not increase the rate of formation, contrary to the slow-phase amplitude. Instead, for the fast-phase amplitude, there is time dependence limiting the reaction.

2.3 PCBM Trimers

PCBM trimers are examined as the potential cause of one of the fast and slow phases, alongside dimers, observed in the thermal decomposition process. GPC measurements were used to probe the kinetics of PCBM trimer formation. Fullerene light exposure can result in high order units such as trimers and oligomers which will affect the bond energy. In C_{60} , the oligomerisation can result in molecules with 21 units.²¹ To determine if this mechanism is responsible for the two-phase kinetics of thermal decomposi-

tion observed the illumination dependence on oligomerisation of PCBM is investigated. Gel permeation chromatography (GPC) eludes the trimer unit faster than the smaller dimer unit (Figure 5). As with the previous absorbance experiments, a select range of radiant exposure and irradiances were used to determine the reaction kinetics of trimerisation. In Figure 5, the trimer signal correlates with radiant exposure (H_e) and is independent of irradiance. This does not follow the trends observed for the formation of the two-phase kinetics where a dependence on irradiance is observed. Furthermore, the fraction of trimer:dimer is determined from the amplitude of each signal in the GPC. The fraction of PCBM trimer to dimer (1:12) does not correlate with the fraction of fast to slow phase (1:4), accounting for reaction stoichiometry. From these observations, it is concluded that PCBM trimerisation does not account for the bi-phase kinetics of decomposition.

2.4 PCBM dimer configurations

Another potential mechanism resulting in the formation of populations of dimers with different bond energies is the configuration of the PCBM dimer bond. The position of the PCBM tail on each of the fullerene units relative to the dimer bond location will affect the bond strength. There are 30 double bonds on a C_{60} cage located at the edge of hexagonal faces of a truncated icosahedron.²¹ These double bonds can undergo the 2+2 cycloaddition reaction to form dimers.²⁸ The symmetry of C_{60} means there is no effect of the dimer bond location on the bond energy. However, due to the asymmetry of PCBM, the location of the dimer bond relative to the PCBM tail will likely affect the associated bond energy. To investigate how significant this effect is density functional theory (DFT) calculations were done on a selection of dimer configurations. On PCBM there are 29 dimer bond locations, excluding the bond with the PCBM tail, resulting in $29 \times 29 = 841$ possible dimer orientations. The asymmetry of the side group means bonds on each configuration will result in different properties.

To effectively investigate the energetic landscape of the possible 841 PCBM dimer configurations a two-step methodology was used. Firstly, the possible bonding sites were split into 8 classes relating to the distance to the PCBM tail, termed β , as depicted in Figure 6(a) and Figure S3. Pre-screening eliminated the class closest to the PCBM tail ($\beta = 1$). For the first step of calculations, the lone bond at class eight was fixed for fullerene-b ($\beta_b = 8$) and this was connected with all 25 bond locations on fullerene-a. All DFT simulations are presented in Figure 6(b) as an individual ring where the size and colour relates to the energy of the bond. From these results, $\beta = 2$ and $\beta = 3$ dimer bond energies are approximately 100 meV higher than the $\beta \geq 4$ configurations, giving a total distribution of 200 meV for $2 \leq \beta \leq 8$. The variation in bond energy should result in a change of reaction constant as defined by an Arrhenius relationship. In the instance where $\Delta E_{a-b} = 0.2$ eV and assuming the equivalent pre-exponential factor then $k_a:k_b = 504$ at 100 °C. Under these conditions, the reaction would be either too slow or too quick and therefore $\beta = 2$ and $\beta = 3$ is assumed to be too unstable and unfeasible. In the instance where $\Delta E_{a-b} = 0.13$ eV as with $\beta \geq 4$ then $k_a:k_b = 57.1$ at 100 °C. This is

remarkably close to the ratio found when modelling the results in Figure 3, where $k_{slow}:k_{fast} = 68.6$ at 100 °C. Therefore the configurations of PCBM dimers with $\beta = 2$ and $\beta = 3$ are energetically unfavourable and thus expected not to form under these conditions. However, energy distribution for dimer configurations at $\beta \geq 4$ are consistent with energies observed experimentally.

For the second step of DFT calculations the remaining configurations with the class of $\beta \geq 4$ are considered. For each class (except $\beta = 8$) there are four bonds meaning a bond between two dimers has 16 possible orientations (i.e. for a dimer between class 7 on dimer a and class 6 on dimer b the possible orientations are $\beta_a:\beta_b = 7_1:6_1, 7_1:6_2, 7_2:6_1$ etc.). In each case only one was considered, except for the most stable configuration, $\beta_a:\beta_b = 4:4$, where six orientations were calculated. Bonds not calculated with DFT calculations were extrapolated from the dimers with equivalent classes. A histogram of all configurations where $\beta \geq 4$ is presented in Figure 6(c). The range of energies is >0.1 eV and therefore significant within the range of temperatures used in this studied.

The correlation between the class, β , and bond energy is considered to understand the origins of the distribution in dimer bond energies. In Figure 6(c), bonds at $\beta = 4$ and $\beta = 6$ are the more stable, and specifically $\beta_B:\beta_A = 4:4$ is the most stable. Surprisingly, class eight is not as stable. When a bond is formed with the fullerene cage it distorts the sphere.^{29,30} This results in increased strain across the cage. If bonds on the fullerene are at opposite sides the distortion will be increased and the strain on the cage will be exaggerated. However, if the bonds are adjacent the distortion and strain is minimized. At bond positions where $\beta = 4$ both the steric hindrance of the side chain is minimized and the distortion of the fullerene cage is minimized.

Inspection of the energy landscape for dimer formation suggests that configurations at class $\beta=4$ and 6 yield the lowest energies, and that substitutions near the fullerene tail are energetically unfavourable and thus unlikely to occur. We tentatively assign the bi-exponential behaviour observed experimentally with two configuration classes, combining DFT estimates and relative topological dimerization requirements between PCBM molecules. Excluding sites (1-3) adjacent to the tail, we hypothesize that two populations comprise sites around the equatorial plane (most favourable energetically) those near the antipode of the tail. It is thus likely that the activation energy associated to PCBM thermal decomposition, previously estimated as 0.96 eV¹⁸, is thus a weighted average $\langle E_a \rangle$ of the site distribution revealed in the present work. Given the DFT energy range computed as approximately $\Delta E_a \simeq 0.10$ eV and our experimental decay rates, we estimate that the two populations exhibit $E_{a,slow} \simeq 0.9$ eV and $E_{a,fast} \simeq 1$ eV, compatible with our observations.

To determine the dominating factor of bond stability the variation of bond energies between classes (i.e. $\beta_a:\beta_b = 4:4, 4:5, 4:6$ etc.) are compared to the variation of bond energies between the same class, but at different orientations (i.e. $\beta_a:\beta_b = 4_1:4_1, 4_1:4_2, 4_1:4_3$ etc.). The most stable class, $\beta = 4$, has greater variability still as two bonds are perpendicular and two parallel, with respect to PCBM tail. Six configurations of $\beta_A:\beta_B = 4:4$ dimers are simulated in Figure S4. The bond energies of these are

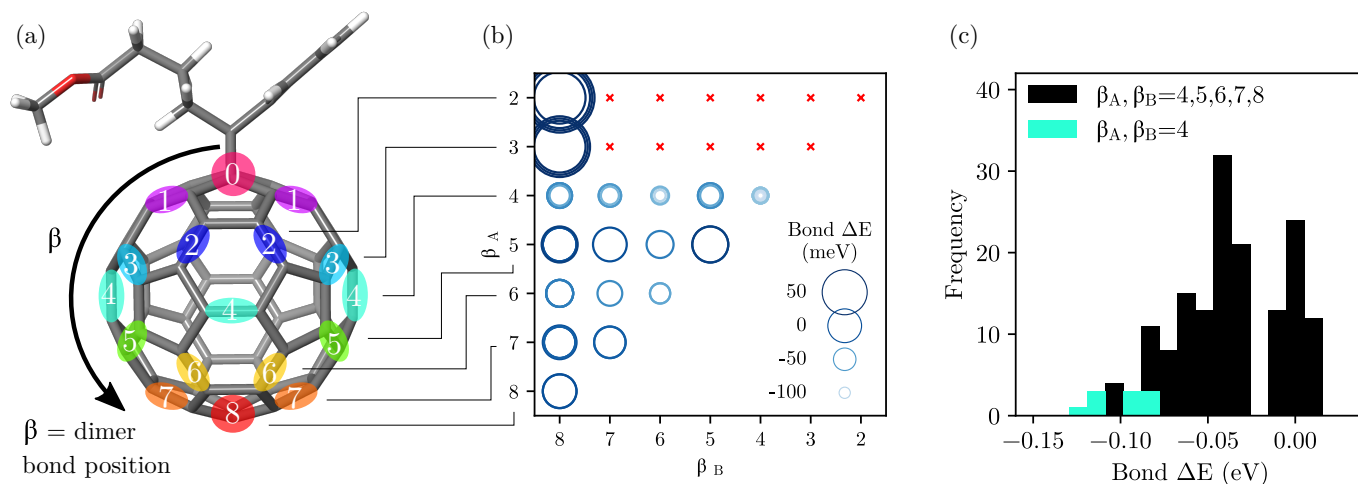


Figure 6 DFT calculations of the possible PCBM dimer configurations. (a) Dimerisation sites occur at double bonds between hexagonal faces. There are eight classes of equivalent distance from the PCBM tail unit. (b) The PCBM dimer bond energy dependence on the class on each fullerene; namely β_A and β_B . Each ring represents a different DFT calculation noting that for each $\beta_A : \beta_B$ point there are 16 orientations due to the asymmetry of the side group (examples are in Figure S4). Both the size and colour of each ring represent the bond energy relative the $\beta_A : \beta_B = 8$ configuration. (c) A histogram of the bond energies of all possible dimer configurations. The $\beta_A : \beta_B = 4$ dimers are the most stable and the spread is not as significant compared to the class, β . Thus the class (β) is a greater factor than the orientation of the PCBM tail of each fullerene.

highlighted in the histogram in Figure 6(c) and given in Table S1. Although the dimers are topologically very different the effect on bond energy is less significant. This is not unexpected as changing the bond orientation might have little effect on the strain experienced by the cage. From these results the dimer bond position relative to the PCBM tail, β , is the dominant factor in determining the bond energy of the dimer. In addition, the formation energy of dimer 8:8 was calculated to be +28 meV, which is less stable than the dimer formation set to a reference value of zero. This can be explained considering that on the one hand, two new bonds are created, but on the other hand some of the fullerene aromaticity is lost, and since these are antagonist effects, it explains the positive energy of formation required. To gain insight into this apparent anomaly, aromaticity analysis was performed. The NICS(0) indexes of the rings involved in the bond creations became strongly antiaromatic. In detail, from values of -2.90 and -2.97 for a single PCBM to values of +3.77 and 5.96 for position 8 (negative values mean aromaticity, positive antiaromaticity). This aromaticity lost sheds light into the positive formation energy obtained for position 8:8.

Finally, to understand the effect of PCBM dimer configuration on device performance the variations on frontier molecular orbitals (FMO) are considered. Figure 7 reports the HOMO and LUMO energy values compared to the dimer bond energy of formation. The HOMO and LUMO energies of the PCBM molecule calculated with these simulation conditions, at -5.57 eV and -3.00 eV, respectively, are considered as a reference. The lines are least-squares error fits to the data. As for the previous analysis, a strong correlation is obtained between the bond formation energy and the FMO energy. A stabilization of the HOMO and LUMO with greater dimer bond energy was found. This is directly related to the fact that the higher the stability of a molecule, the deeper the electronic levels of the HOMO, which corresponds to a gain in electronic energy. From these results, it is concluded the

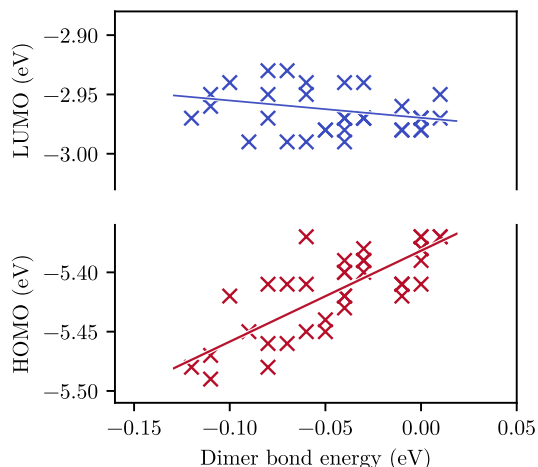


Figure 7 The effect of PCBM dimerisation on the frontier molecular orbital levels as calculated by DFT simulations. The stabilization of the dimer bond energy results in the widening on the band gap. Dimerisation results in the increased disorder of both the HOMO and LUMO level. The solid lines present fits with the least-squares error.

dimer bond energy will affect the electronic properties of PCBM.

3 Discussion

Previous studies have shown PCBM dimerisation to correlated with both beneficial and detrimental effects on stability. Typically, studies presenting the preferential effect of PCBM dimerisation are performed at low light irradiance (≈ 0.1 Sun). However, studies demonstrating the degradation induced by dimerisation are performed at higher light irradiance (≈ 1 Sun). Here it is shown that the irradiance affects the formation of the dimer con-

figuration and, subsequently, the molecular orbital levels. At high light intensities, a larger proportion of strongly-bound dimers are formed. These dimers are calculated to have a LUMO level 2-3 kT greater than that of PCBM and as such effect the mobility of polarons through PCBM. At lower light intensities greater weakly-bound dimers are formed which have a LUMO approximately equal the PCBM monomer. With this understanding, it is possible to comprehend the double-edged effects of dimerisation.

The formation of the fast- and slow-phase of the de-dimerisation has different photophysical mechanisms. The fast phase of weakly-bound dimers was time-dependent whilst the slow phase of strongly-bound dimers was irradiance dependent. This is likely due to the matrix constraining the orientation of the weak dimers such that the correct alignment occurs infrequently. Interpreting the formation of strong and weak dimers with these mechanisms allows for the comprehension of the irradiance dependence of dimerisation. At higher irradiance, dimers are saturated in the strong configuration before weak dimers are formed. Whilst at lower irradiance, dimers are able to form in both weak and strong configuration. The different factors limiting the weak and strong dimerisation results in an irradiance dependence of formation.

The dominant PCBM dimerisation mechanism during the operation of a solar cell will be greatly affected by the location. To predict the overall beneficial or detrimental effects of dimerisation it is important to consider the diurnal and annual irradiance variation. A solar cell is likely to exhibit the greatest thermal stress whilst at high light intensities. The beneficial effects of morphological stability under thermal stress will only be experienced under high light intensity resulting in strongly-bound dimers. Additionally, the cyclic conditions will result in the equilibrium tending towards the most stable strongly-bound dimer. Therefore, under operating conditions of a solar cell it may be unavoidable not to form the detrimental strongly-bound dimers that have been associated with 'burn-in'.

4 Conclusions

This work rationalizes the reasons for the double-edged effects of PCBM dimerisation previously reported in the literature. By investing the de-dimerisation kinetics upon thermal annealing two populations of dimers have been found to form. Photodimerisation at high irradiance is shown to result in strongly-bound dimers whilst at lower irradiance weakly-bound dimers are also formed. DFT calculations suggest the origin of this energetic distribution in dimer bond energy originates in the location of the PCBM tail with respect to the dimer bond on the fullerene cage. The simulations also show the dimer bond energy is correlated with molecular orbital levels. The ideas presented enable a pathway to comprehend to varied effects of PCBM dimerisation on device stability.

5 Experimental Section

Sample preparation. Solutions of phenyl-C61-butyric acid methyl ester, PCBM, supplied by Nano-c and poly[N-9'-heptadecanyl-2,7-carbazole-alt-5,5-(4',7'-di-2-thienyl-2',1',3'-benzothiadiazole)], PCDTBT, supplied by 1-materials were prepared at a combined

concentration of 25 mg mL⁻¹ in chlorobenzene. Glass substrates were plasma treated in an oxygen atmosphere with a Emitech K1050X before solutions of 1:2 PCDTBT:PCBM were spin coated at 1500 rpm for 30 s. The resulting film thicknesses was \approx 100 nm, measured by stylus profilometry (Dektak XT). For the GPC measurements the samples were re-dissolved in chlorobenzene.

Illumination and annealing was carried out in a nitrogen filled glovebox with oxygen and humidity levels kept < 15ppm. A Bridgelux 4000 K white LED light source was used with the spectrum previously reported.¹⁹ For thermal stress, temperatures were controlled with a hotplate or cooling plates and calibrated with an IR temperature sensor in the presence of the illumination to ensure accurate temperature control.

UV-visible absorption spectroscopy was carried out with a Shimadzu UV-1601 spectrophotometer. Measurements were taken from 300 nm to 350 nm in transmission mode. To determine an assay of PCBM dimer concentration the absorbance was normalised to a peak at \approx 340 nm and the change at the peak minimum at \approx 320 nm monitored.

Density functional theory (DFT) simulations were optimised with B3LYP functional and the 6-31G(d) Pople's basis set. To study all possible dimer conformations and to take into account the symmetry of the system, two steps have been considered. In the first, one bond was considered fixed and one by one all the possible dimers with the other PCBM have been created. Next, considering the most stable sites obtained from the first step, new dimers have been created and conformations analysed. Since it is not possible to computationally study all the 689 possible configurations, only selected ones have been considered, for a total of 49 dimers. To calculate the aromaticity of the rings forming PCBM before and after the dimer formations, the NICS indexes have been considered. A single point energy calculation was performed on the selected PCBM and position 8 considering the centre of all rings (NICS(0)) and at the centre of the PCBM sphere.

Gel permeation chromatography with in-situ optical measurements were performed using an Agilent Technologies 1260 Infinity GPC System with 1260 RID and DAD VL attachments. Measurements were performed at 80 °C, using analytical grade chlorobenzene as eluent with two PLgel 10 μ m MIXED B columns in series. Samples were prepared using analytical grade chlorobenzene in concentrations of 1 mg mL⁻¹ to 2 mg mL⁻¹ and filtered with VWR PES membrane 0.45 μ m syringe filters before submission. An injection volume of 50 μ L and GPC flow rate of 1.00 mL min⁻¹ was used. The absorbance at 300 nm, 320 nm, and 335 nm were used to monitor the elution and found to give equivalent results.

6 Supporting Information

Supporting Information is available...

7 Acknowledgements

We thank the Engineering and Physical Sciences Research Council (EPSRC, UK, EP/L016702/1) and Solvay for financial support. Data presented in this paper are available on the Zenodo repository at...

References

- 1 S. A. Gevorgyan, M. V. Madsen, B. Roth, M. Corazza, M. Hösel, R. R. Søndergaard, M. Jørgensen and F. C. Krebs, *Advanced Energy Materials*, 2016, **6**, 1501208.
- 2 J. Zhao, Y. Li, G. Yang, K. Jiang, H. Lin, H. Ade, W. Ma and H. Yan, *Nature Energy*, 2016, **1**, 15027.
- 3 S. Zhang, L. Ye and J. Hou, *Advanced Energy Materials*, 2016, **6**, 1–20.
- 4 W. Zhao, S. Li, H. Yao, S. Zhang, Y. Zhang, B. Yang and J. Hou, *Journal of the American Chemical Society*, 2017, **139**, 7148–7151.
- 5 L. Meng, Y. Zhang, X. Wan, C. Li, X. Zhang, Y. Wang, X. Ke, Z. Xiao, L. Ding, R. Xia, H.-L. Yip, Y. Cao and Y. Chen, *Science*, 2018, **4**, eaat2612.
- 6 H. K. H. Lee, A. M. Telford, J. A. Röhr, M. F. Wyatt, B. Rice, J. Wu, A. de Castro Maciel, S. M. Tuladhar, E. Speller, J. McGettrick, J. R. Searle, S. Pont, T. Watson, T. Kirchartz, J. R. Durrant, W. C. Tsoi, J. Nelson and Z. Li, *Energy & Environmental Science*, 2018, **11**, 417–428.
- 7 W. R. Mateker and M. D. McGehee, *Advanced Materials*, 2017, **29**, 1603940.
- 8 I. Fraga Domínguez, A. Distler and L. Lüer, *Advanced Energy Materials*, 2017, **7**, 1601320.
- 9 M. Jørgensen, K. Norrman, S. A. Gevorgyan, T. Tromholt, B. Andreasen and F. C. Krebs, *Advanced Materials*, 2012, **24**, 580–612.
- 10 S. Savagatrup, A. D. Printz, T. F. O'Connor, A. V. Zaretski, D. Rodriguez, E. J. Sawyer, K. M. Rajan, R. I. Acosta, S. E. Root and D. J. Lipomi, *Energy Environ. Sci.*, 2015, **8**, 55–80.
- 11 P. Cheng, C. Yan, Y. Wu, J. Wang, M. Qin, Q. An, J. Cao, L. Huo, F. Zhang, L. Ding, Y. Sun, W. Ma and X. Zhan, *Advanced Materials*, 2016, **28**, 8021–8028.
- 12 W. Chen, M. P. Nikiforov and S. B. Darling, *Energy & Environmental Science*, 2012, **5**, 8045.
- 13 H. Kang, W. Lee, J. Oh, T. Kim, C. Lee and B. J. Kim, *Accounts of Chemical Research*, 2016, **49**, 2424–2434.
- 14 A. Guerrero and G. Garcia-Belmonte, *Nano-Micro Letters*, 2017, **9**, 10.
- 15 A. Distler, T. Sauer mann, H.-J. Egelhaaf, S. Rodman, D. Waller, K.-S. Cheon, M. Lee and D. M. Guldi, *Advanced Energy Materials*, 2014, **4**, 1300693.
- 16 T. Heumueller, W. R. Mateker, A. Distler, U. F. Fritze, R. Cheacharoen, W. H. Nguyen, M. Biele, M. Salvador, M. von Delius, H.-J. Egelhaaf, M. D. McGehee and C. J. Brabec, *Energy Environ. Sci.*, 2016, **9**, 247–256.
- 17 Z. Li, H. C. Wong, Z. Huang, H. Zhong, C. H. Tan, W. C. Tsoi, J. S. Kim, J. R. Durrant and J. T. Cabral, *Nature communications*, 2013, **4**, 1–7.
- 18 H. C. Wong, Z. Li, C. H. Tan, H. Zhong, Z. Huang, H. Bronstein, I. McCulloch, J. T. Cabral and J. R. Durrant, *ACS Nano*, 2014, **8**, 1297–1308.
- 19 S. Pont, F. Foglia, A. M. Higgins, J. R. Durrant and J. T. Cabral, *Advanced Functional Materials*, 2018, **1802520**, 1802520.
- 20 L. N. Inasaridze, A. I. Shames, I. V. Martynov, B. Li, A. V. Mumyatov, D. K. Susarova, E. A. Katz and P. A. Troshin, *J. Mater. Chem. A*, 2017, **5**, 8044–8050.
- 21 A. Rao, K.-A. Wang, J. Holden, Y. Wang, P. Zhou, P. Eklund, C. Eloi and J. Robertson, *Journal of Materials Research*, 1993, **8**, 2277–2281.
- 22 Y. Wang, J. Holden, Z.-H. Dong, X.-X. Bi and P. Eklund, *Chemical Physics Letters*, 1993, **211**, 341–345.
- 23 A. Dzwilewski, T. Wågberg and L. Edman, *Journal of the American Chemical Society*, 2009, **131**, 4006–4011.
- 24 A. Distler, *PhD thesis*, University of Erlangen-Nuremberg, 2015.
- 25 C. Keiderling, S. Dimitrov and J. R. Durrant, *The Journal of Physical Chemistry C*, 2017, **121**, 14470–14475.
- 26 Y. Wang, J. Holden, X.-x. Bi and P. Eklund, *Chemical Physics Letters*, 1994, **217**, 413–417.
- 27 P. Eklund, A. Rao, P. Zhou, Y. Wang and J. Holden, *Thin Solid Films*, 1995, **257**, 185–203.
- 28 S. G. Stepanian, V. A. Karachevtsev, A. M. Plokhotnichenko, L. Adamowicz and A. M. Rao, *The Journal of Physical Chemistry B*, 2006, **110**, 15769–15775.
- 29 G. B. Adams, J. B. Page, O. F. Sankey and M. O'Keeffe, *Physical Review B*, 1994, **50**, 17471–17479.
- 30 M. Suzuki, T. Iida and K. Nasu, *Physical Review B*, 2000, **61**, 2188–2198.

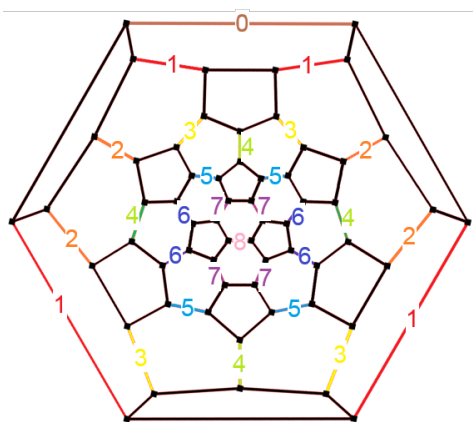


Figure S3 The Schlegel projection of a truncated icosahedron presenting the PCBM dimer bond locations investigated with this study, β . The dimerisation occurs on a double bond located between two hexagonal faces. The value β indicates bond positions of equivalent distance to the reference bond at $\beta = 0$

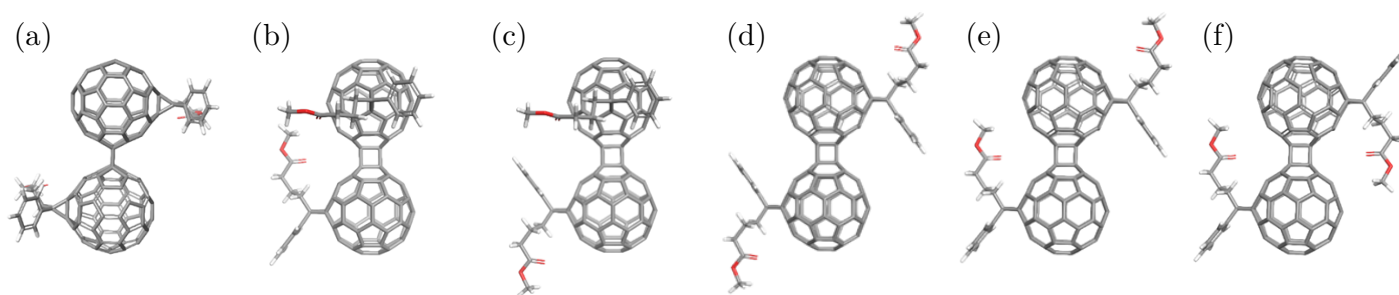


Figure S4 Possible $\beta_A : \beta_B = 4 : 4$ bond orientations calculated with DFT simulations. Note the $\beta = 4$ bond position has two orientations; either vertical or horizontal with respect the PCBM tail, as shown in Figure 6. Therefore the range of configurations is diverse.

Table S1 Calculated bond energies for simulated dimers with a $\beta_A : \beta_B = 4 : 4$ configuration, as shown in Figure S4.

DFT simulation in Figure S4	(a)	(b)	(c)	(d)	(e)	(f)
Bond ΔE (meV)	-0.09	-0.11	-0.08	-0.12	-0.11	-0.08